[Frontiers in Bioscience 13, 1371-1384, January 1, 2008]

Physical principles of quantitative nuclear magnetic resonance oximetry

Vikram D. Kodibagkar[1], Xianghui Wang[1] , Ralph P. Mason[1]

[1]Cancer Imaging Program, Department of Radiology, UT Southwestern, Dallas TX

TABLE OF CONTENTS

1. ABSTRACT

Over the years many techniques have been devised for the measurement of tissue oxygenation (oximetry). Oximetry using polarographic needle electrodes has long been considered a gold standard. Nuclear Magnetic Resonance (NMR) based oximetry uses exogenously administered reporter molecules such as perfluorocarbons to quantitatively interrogate oxygen tension (pO_2). This technique has been successfully used *in vivo* in the preclinical setting and shows promise for clinical applications. NMR pO_2 reporter molecules display a linear dependence of the spin lattice relaxation rate on pO_2, which forms the basis of this technique. Physical principles of spin lattice relaxation of pO_2 reporter molecules and the pO_2 dependence of relaxation rate are discussed in this review. Practical considerations for choice of reporter molecules for *in vivo* measurements, general methodology and new developments are also described.

2. INTRODUCTION

2.1. Tissue oxygenation and hypoxia

Oxygen is essential for tissue health and any reduction in its supply can lead to rapid cellular dysfunction and cell death. It is also an important variable in the treatment of many medical conditions including tumors, peripheral vascular disease, and stroke. In solid tumors, oxygen delivery is impaired by structural abnormalities present in the tumor vasculature such as chaotic vessel architecture. In addition, the altered tumor cell metabolism with elevated metabolic rates contributes to the occurrence of low tissue oxygenation (hypoxia). Hypoxia can adversely affect the efficacy of radiation therapy, chemotherapy, and photodynamic therapy (1). These therapies rely on creation of reactive oxygen species, which can kill cancer cells by damaging DNA and sub cellular organelles (2). Reactive oxygen species are also formed as a natural byproduct of normal metabolism of

oxygen and have important roles in cell signaling (3). Production of reactive oxygen species from molecular oxygen by macrophages and neutrophils probably plays a key role in cell-mediated immunity and microbiocidal activity (4). Measurements of pO_2 in tumors have been found to have prognostic value and the probability of disease-free survival is significantly lower for patients with hypoxic tumors (5-8). Given the importance of oxygen, the ability to measure tissue oxygen tension non-invasively may have a significant impact in understanding mechanisms of tissue function and in clinical prognosis of disease. Quantitative tissue oximetry remains a challenge, especially *in vivo* and this review will consider progress in magnetic resonance approaches and the physical foundations underpinning the method.

2.2. Measurement of tissue oxygenation

Many techniques have been used to assess tissue oxygenation *in vivo*, both qualitative and quantitative as reviewed extensively (1, 9, 10). Direct measurement methods include those using electrodes and fiber-optic probes. These methods have been used for *in vivo* research and also in the clinical setting, but are invasive and may be unsuitable for routine human use. Indirect methods such as those based on Magnetic Resonance (MR) measure parameters that report on local oxygenation status (see section 3).

Measurements of pO_2 using polarographic needle electrodes have long been considered a gold standard (1, 11, 12). Typically, an anode is placed on the skin and polarized with a constant voltage. The polarographic needle electrode (cathode) consists of a gold filament embedded within a flexible stainless steel housing with an oxygen permeable membrane covering the opening. The cathode is inserted into the tissue of interest and electrical current is generated at the tip of the electrode, which is proportional to the tissue oxygen pressure. Polarographic electrodes are calibrated in phosphate buffered normal saline, bubbled with gases with a range of pO_2s. Multiple electrodes may be placed at different locations in tissue in order to measure spatial heterogeneity and one can make dynamic measurements to gauge the response to intervention (13). The invasiveness of this technique can be minimized by use of electrode tips as fine as a few microns (14), but these are fragile and are susceptible to stray electromagnetic fields. The Eppendorf Histograph is an improved version of this technique that can make multiple successive measurements along tracks in tissue using a stepwise motion of the needle electrode under computer control (15). It has been successfully used in the clinical setting and revealed hypoxia in many tumor types that are externally accessible (6-8, 12, 16-19). The drawbacks of polarographic electrodes are that measurements can be affected by changes in pH, salinity, and ionic strength. Electrodes also consume oxygen, and thus, may bias readings especially under hypoxic conditions (such as found in tumors) and over long measurement periods.

Another quantitative method for measuring the partial pressure of dissolved or gaseous oxygen utilizes fiber-optic oxygen sensors based on fluorescence. Typically, an optical fiber carries excitation light to the fluorophore coating at the probe tip. Fluorescence generated at the tip is returned by the optical fiber to a spectrometer. When oxygen in the gas or liquid sample diffuses into the fluorophore coating, it quenches the fluorescence. Commercial instruments exploit various parameters such as fluorescence lifetime (OxyLite™) or relative fluorescence intensity (FOXY™), which are correlated with pO_2, and hence, a calibration curve can be used to measure pO_2 *in vivo*. The fluorophores used in commercial systems may be platinum based (OxyLite™) or ruthenium based (FOXY™). This method does not consume oxygen during measurement, but the fluorophore coating may wear off after several measurements and needs to be re-applied to the fiber. Weak detected fluorescence intensity is a clear sign that fluorophore coating needs to be re-applied. Probes can be coated with oxygen permeable coatings to further protect the fluorophore. This usually slows the response time of measurement. Several recent applications have been reported (20-31). Fiber optic probes are more fragile than the Eppendorf Histograph.

Qualitative methods have been used to non-invasively identify tumor regions that are hypoxic based on selective accumulation of specially designed reporter molecules in such regions (32). Following intravenous infusion, these reporter molecules are trapped in tissues in the absence of oxygen, very much like molecules such as pimonidazole and EF5 that are widely used in histological assessment of hypoxia (33). Many such reporter molecules have been developed for different modalities such as NMR (34-36), positron emission tomography (PET) (37-40) and single photon emission computed tomography (SPECT) (41, 42). The red shift of the fluorescence of green fluorescent protein (GFP) under hypoxic conditions has also been used to image hypoxia by fluorescence imaging (43). Exploiting various biochemical pathways that are under oxygen regulation such as induction of hypoxia-inducible factor 1 (HIF-1) or introduction of transgenes with hypoxic response elements (HREs) coupled to reporter genes has enabled the visualization of hypoxia by optical imaging (44-47).

2.3. Magnetic Resonance in Bioscience

In biomedicine, the abundant hydrogen nuclei from tissue water can be utilized to obtain high-resolution anatomical images using Magnetic Resonance Imaging (MRI) to probe living systems non-invasively. Of all medical imaging modalities, MRI provides the best combination of spatial and temporal resolution to yield superb anatomical detail and functional information. It has become an invaluable clinical tool for diagnosis of many diseases. Using tricks of nuclear spin physics it is possible to obtain information beyond structural anatomy. Routinely, one can study diverse aspects of physiology, such as vasculature and blood flow (48-50), cellularity and apparent diffusion (51-54), vascular and tissue oxygenation (9, 55-59) as well as tissue perfusion and endothelial permeability (60, 61). The development of contrast agents and reporter molecules has pushed the limits of detection and established MRI as a tool for molecular imaging (62-64). Assessment of key metabolites such as lactate, choline

and N-acetyl aspartate (NAA) by proton NMR has enabled the assessment of metabolic changes at onset of disease (65-71).

Magnetic Resonance (MR) based techniques to measure oxygenation may be divided into quantitative and qualitative methods. Qualitative MR techniques, such as BOLD (Blood Oxygen Level Dependant) contrast use blood oxygenation status as a surrogate marker for tissue oxygenation. BOLD can provide high spatial and temporal resolution and can assess dynamic changes in vascular oxygenation using endogenous deoxyhemoglobin, and is the basis for functional MRI. For large blood vessels where imaging voxels are wholly within a vessel quantitative oximetry has been reported (55, 72, 73). However, since BOLD contrast (changes in T_2*) depends on the amount of deoxyhemoglobin it is influenced by hematocrit, vascular volume, pH and flow. While signal changes are sensitive to changes in vascular oxygenation, the relationship with tissue pO_2 is neither straightforward nor direct in tissues (58). Quantitative MR oximetry techniques have been developed based on reporter molecules for nuclear magnetic resonance (NMR) (9, 74-76) and electron paramagnetic resonance (EPR) (10, 77-81). EPR is a technique that is very similar to NMR in that they both result from the Zeeman interaction of a spin with an external magnetic field. Unlike NMR where nuclei like protons with non-zero nuclear spin give rise to the signal, EPR relies on unpaired electrons. EPR oximetry, much like NMR oximetry, relies on the indirect methods that exploit the paramagnetic properties of molecular oxygen. Paramagnetic oxygen not only relaxes nuclear spins, but also is effective in electronic T_1 and T_2 relaxation of other paramagnetic species or radicals. The EPR linewidth of the radical is broadened and the change in the relaxation rate is often proportional to the concentration of oxygen over a wide range of oxygen tensions. Similar to NMR oximetry, *in vivo* EPR oximetry also requires prior intravenous or intramuscular infusion of free radicals, or direct implantation of particulate spin probes into the tissue of interest. This technique has been reviewed extensively elsewhere (81, 82). The method can offer exceptional sensitivity at very low pO_2 values. A primary shortcoming is the lack of widespread EPR instrumentation for small animal investigations, l*et al*one clinical studies.

Although extensive reviews exist on NMR oximetry (9, 76), they have generally focused on applications. Here, we focus on the underlying physical principles. NMR based oximetry uses exogenously administered reporter molecules to interrogate oxygen tension (pO_2). Such exogenous agents, which can quantitatively report tissue oxygenation, have been successfully used *in vivo* in the preclinical setting. NMR pO_2 reporter molecules are often perfluorocarbons, which display a linear dependence of the ^{19}F spin lattice relaxation rate R_1 (=$1/T_1$) on pO_2. We will also describe an analogous ^1H NMR approach using a recently identified ^1H pO_2 reporter molecule hexamethyldisiloxane (83).

3. NMR AND MRI OXIMETRY

3.1. Dependence of spin lattice relaxation rate of reporter molecules on pO_2

Molecular oxygen is paramagnetic and therefore tends to shorten nuclear spin-lattice relaxation times, T_1 and T_2, in solution or *in vivo*. Most of the NMR oximetry applications utilize the linear dependence of the ^{19}F longitudinal (spin-lattice) relaxation rate (R_1=$1/T_1$) of fluorine nuclei of perfluorocarbons (PFC) on the partial pressure of oxygen (9, 84, 85). PFCs exhibit specific characteristics that are critical for *in vivo* oximetry: high oxygen solubility and hydrophobicity. Hydrophobicity ensures the exchange of gases between the PFC and surrounding tissue, while preventing the exchange of aqueous ions, which could perturb R_1. The linear dependence of PFC R_1 on pO_2 can be understood as follows. One can visualize two types of PFC molecules in the PFC pool, those with and without oxygen in their vicinity. If those free of oxygen have a **diamagnetic** longitudinal relaxation rate of R_{1d}, the ones with oxygen in their immediate vicinity have a longitudinal relaxation rate of $R_{1d} + R_{1p}$, where R_{1p} is the **paramagnetic** contribution of oxygen. Since the oxygen molecules rapidly diffuse in the solvent, the observed relaxation rate for each type of fluorine atom is a molar weighted average:

$$R_1 = (1-x)\, R_{1d} + x\,(R_{1d} + R_{1p}) = R_{1d} + x*R_{1p} \quad (1)$$

where x is the mole fraction of oxygen. Since PFCs behave as essentially ideal liquids, the solubility of oxygen in the PFCs obeys Henry's law,

$$pO_2 = k*x \quad (2)$$

where k is a constant that reflects solubility of oxygen in the PFC. It is therefore different for different PFCs. Combining eqs. 1 and 2

$$R_1 = R_{1d} + pO_2*R_{1p}/k \quad (3)$$

Thus, the plot of R_1 vs. pO_2 at a given temperature should be linear, with an intercept of R_{1d} and a slope of R_{1p}/k. R_{1d} is the anoxic relaxation rate, *i.e*., the relaxation rate in absence of oxygen, and R_{1p} is the relaxation rate due to the paramagnetic contribution of oxygen dissolved in the solution or tissue.

3.2. Diamagnetic contributions to R_1

The diamagnetic contribution R_{1d} to the total relaxation rate of PFCs generally results from a combination of ^{19}F-^{19}F dipole-dipole (DD) interactions and ^{19}F chemical-shift anisotropy (CSA) at high magnetic fields. When molecular motions are in the extreme narrowing region the DD contribution to R_{1d} (R_{1DD}) is independent of the magnetic-field strength (86), but the CSA contribution to R_{1d} (R_{1CSA}) varies directly as the square of the magnetic-field strength (87). Thus, at relatively low magnetic fields, the CSA contribution to relaxation is negligible, while at high

magnetic fields it is comparable to the contribution of DD interactions. In general, we can treat DD and CSA interactions as independent and additive contributions to R_{1d}, but they can be correlated in some cases. DD and CSA interactions within a CF_2 or CF_3 group can interfere with each other because they both are fixed to the same physical structure and this correlation can cause the relaxation curve to be multi exponential by introducing a slow relaxing component (88-90) in some cases. Generally such effects on R_{1d} are negligible. Any inter-molecular DD contribution can be assimilated into the intramolecular DD contribution and represented by an effective ^{19}F-^{19}F distance r_{FF}. An exact expression for the DD and CSA relaxation times depends on the structure and the molecular dynamics of the functional group under consideration (*i.e.*, CF_3, CF_2, or CF) and can be quite complicated. Some knowledge of the molecular dynamics may allow assumptions to compute an exact expression, which can then be compared with experimental observations. For example, internal rotation of the CF_2 groups in a linear chain PFC may be sterically hindered and considered to be fixed motionless in a rigid sphere that undergoes isotropic rotational diffusion. For the terminal CF_3 group, reorientation results from the same isotropic rotational diffusion of the rigid sphere and random internal 120° jumps about the three-fold symmetry axis fixed in the sphere. It is reasonable to assume that the principle component of the chemical shift tensor lies along the C-F bond and one can use chemical-shielding anisotropy ($\Delta\sigma$) and asymmetry (η_σ) values from literature. Such internal motion will lead to extra terms and the angular dependence in the equations for the CF_3 group compared to the CF_2 group. Shukla *et al.* (91) calculated the DD and CSA relaxation rates for the CF_2 and CF_3 groups of perfluorotributylamine (PFTB) and compared theory with experimental measurements of R_{1a} (= R_{1DD} + R_{1CSA}). For the CF_2 group,

$$R_{1DD} = \frac{(N-1)3\gamma^4\hbar^2}{10{r_{FF}}^6}\left[j_1(\omega_0) + 4j_2(2\omega_0)\right] \quad (4)$$

$$R_{1CSA} = \frac{2(\gamma B_0 \Delta\sigma)^2}{15}\left(1 + \frac{{\eta_\sigma}^2}{3}\right) j_1(\omega_0) \quad (5)$$

while for the CF_3 groups,

$$R_{1DD} = \frac{(N-1)3\gamma^4\hbar^2}{10{r_{FF}}^6} \times \left\{ \left[\frac{1}{4}(3\cos^2\Delta_{DD} - 1)^2 \right] \left[j_1(\omega_0) + 4j_2(2\omega_0) \right] + \left[1 - \frac{1}{4}(3\cos^2\Delta_{DD} - 1)^2 \right] \left[j_{1j}(\omega_0) + 4j_{2j}(2\omega_0) \right] \right\} \quad (6)$$

$$R_{1CSA} = \frac{2(\gamma B_0 \Delta\sigma)^2}{15}\left(1 + \frac{\eta_\sigma^2}{3}\right) \left\{ \left[\frac{1}{4}(3\cos^2\Delta_{CSA} - 1)^2 \right] j_1(\omega_0) + \left[1 - \frac{1}{4}(3\cos^2\Delta_{CSA} - 1)^2 \right] j_{1j}(\omega_0) \right\} \quad (7)$$

where N is the number of ^{19}F nuclei in the group (2 for CF_2 and 3 for CF_3), γ is the gyromagnetic ratio of ^{19}F, B_0 is the spectrometer magnetic-field strength and ω_0 is the corresponding ^{19}F Larmor frequency (= γB_0). Δ_{DD} is the angle between the F-F vector and the internal rotation axis and Δ_{CSA} is the angle between the principle axis of the chemical-shift tensor and the internal rotation axis. The spectral density functions $j_n(n\omega_0)$ and $j_{nj}(n\omega_0)$ are related to the correlation times of isotropic rotational diffusion of the molecule (τ_c) and internal rotation of the CF_3 group around the symmetry axis (τ_{ci}), respectively, by

$$j_n(n\omega_0) = \frac{\tau_c}{1 + (n\omega_0\tau_c)^2} \quad (8)$$

$$j_{nj}(n\omega_0) = \frac{\tau_{cj}}{1 + (n\omega_0\tau_{cj})^2} \quad (9)$$

where

$$1/\tau_{ci} = 1/\tau_c + 1/\tau_{ci} \quad (10)$$

Assuming that all bond angles for the CF_3 groups are tetrahedral (Δ_{DD}=90°, Δ_{CSA}= 71°),
eqns. 6 and 7 reduce to

$$R_{1DD} = \frac{3\gamma^4\hbar^2}{5{r_{FF}}^6} \times \left\{ 0.25\left[j_1(\omega_0) + 4j_2(2\omega_0) \right] + 0.75\left[j_{1j}(\omega_0) + 4j_{2j}(2\omega_0) \right] \right\} \quad (11)$$

$$R_{1CSA} = \frac{2(\gamma B_0 \Delta\sigma)^2}{15}\left(1 + \frac{\eta_\sigma^2}{3}\right) \left\{ 0.11 j_1(\omega_0) + 0.89 j_{1j}(\omega_0) \right\} \quad (12)$$

In the motional narrowing limit $j_n(n\omega_0) \rightarrow \tau_c$ and $j_{nj}(n\omega_0) \rightarrow \tau_{ci}$, and further simplification of the above equations is possible. The relative contributions of DD and CSA to R_{1d} can vary with temperature and magnetic field. In the case of perfluorotributylamine (PFTB), R_{1CSA} was found to be greater than R_{1DD} for CF_2 groups at high fields, while R_{1DD} dominates over R_{1CSA} for the CF_3 group (91). Internal molecular rotation of the CF_3 group results in a greater fractional decrease in R_{1CSA} compared to the fractional decrease in R_{1DD}. From eqns. 4, 5, 11 and 12, in the limit where internal rotation is extremely fast (*i.e.*, τ_{ci}, $\tau_{cj} \rightarrow 0$), $R_{1DD}(CF_3) = R_{1DD}(CF_2)/2$ and $R_{1CSA}(CF_3) = R_{1CSA}(CF_2)/9$.

The anoxic contribution to the relaxation rate, R_{1d}, represents the lower limit of R_1 with respect to pO_2 reporter molecules. Accurate determination is essential for calibration, as it represents "0 torr". In the case of a molecule like hexafluorobenzene (HFB), the expression for R_{1DD} will be similar to eqn. 4. However, three different F-F distances must be taken into account. Each F nucleus has two ortho (r_{FF} ~2.91Å), two meta (r_{FF} ~5.04 Å) and one para (r_{FF} ~5.82 Å) F neighbors and the total R_{1DD} will be a sum of these three components. Due to the strong $1/{r_{FF}}^6$ dependence, the para and the meta contributions may be small (1/27 and 1/128 of the ortho

contribution, respectively, accounting for the distances and number of atoms), but this has not been verified. Compared to CF_3 (r_{FF} ~2.41Å) and CF_2 (r_{FF} ~2.38Å) groups the closest FF distance in HFB is larger, and hence, one might expect R_{1DD} to be smaller. Indeed, the anoxic relaxation rate of HFB (~0.08 s^{-1}) is smaller than those of the α-CF_2 (~1.35 s^{-1}) and CF_3 (~0.88 s^{-1}) resonances in PFTB (91, 92). Of course, the differences in R_{1d} for different perfluorocarbons cannot be accounted for by considering the F-F distances only; molecular dynamics and CSA contributions play a major role as well.

3.3. Paramagnetic contribution of oxygen

The presence of dissolved oxygen affects the chemical shift as well as the relaxation rates of the PFC molecules in their vicinity. The measured paramagnetic chemical shift, $\Delta\sigma_P$, in presence of oxygen results from a Fermi contact interaction between molecular oxygen and PFC nuclei and is given by (86, 93)

$$\Delta\sigma_P = \frac{Axn_M hS(S+1)\gamma^2 g_e{}^2 \beta_e{}^2}{g_N{}^2 \beta_N{}^2 kT} \quad (13)$$

where A is the hyperfine constant, x is the mole fraction of oxygen, n_M is the number of PFC molecules surrounding an oxygen molecule, h and k are Planck and Boltzmann constants, γ is the nuclear gyromagnetic ratio, $g_e\beta_e$ and $g_N\beta_N$ are the electron and nuclear magnetic moments, *S* is the total electron spin of the paramagnetic species (S = 1 for O_2), and T is the absolute temperature. Using eqns. 2 and 13 one could try to measure pO_2 from the chemical shift using a predetermined calibration curve. However, $\Delta\sigma_P$ is usually small and is superimposed upon chemical shifts induced by changes in bulk magnetic susceptibility due to the presence of oxygen. Separating the two effects would require the ability to apply B_0 perpendicular, as well as parallel to the sample(93). For *in vivo* imaging, shimming could also affect the measurement of $\Delta\sigma_P$ and this method has not been used to measure pO_2.

The presence of any dissolved oxygen results in a paramagnetic contribution, R_{1p}, which is given by (93, 94)

$$R_{1p} = \frac{2S(S+1)\gamma^2 g^2 \beta^2}{15r^6}\left[\frac{3\tau_c}{1+\omega_I{}^2\tau_c{}^2} + \frac{7\tau_c}{1+\omega_S{}^2\tau_c{}^2}\right] \quad (14)$$

where r is the distance between the paramagnetic center and the nucleus concerned, ω_S is the angular frequency of electron resonance, and ω_I is the angular frequency of nuclear resonance. Here, we ignore the contribution due to contact interaction as oxygen does not form a complex with the PFCs, and hence the hyperfine interaction would be very small. The correlation time for the reorientation of the coupled magnetic moment vectors, τ_c, is given by

$$1/\tau_c = 1/\tau_s + 1/\tau_r + 1/\tau_e \quad (15)$$

where τ_s is the electron spin relaxation time, τ_r, is the rotational correlation time, and τ_e, is the residence time of the paramagnetic species. In the motional narrowing limit, $\omega_S\tau_c << 1$ and $\omega_S\tau_c << 1$ so eqn. 11 simplifies to

$$R_{1p} = \frac{8\gamma^2 g^2 \beta^2 \tau_c}{3r^6} \quad (16) \text{ for S=1.}$$

R_{1p} determines the sensitivity of the PFC spin lattice relaxation rate to the presence of oxygen. PFCs with multiple ^{19}F atoms (with unique chemical shifts) generally exhibit a different R_1 response of each resonance to pO_2 (*i.e.*, different slopes on an R_1 vs. pO_2 graph). These differences are a result of the inverse dependence of R_{1p} on r^6 and imply that oxygen has a preferred approach to each PFC molecule. If the average distances between the oxygen molecule and various fluorine atoms in a PFC are different, R_{1p} would be larger for the fluorine nuclei that are closer to the oxygen molecule. Effective spin diffusion within the molecule can lead to the reduction of differences in the slopes. The preferences of the approach of oxygen to different parts of the PFCs are most likely due to steric factors rather than specific binding as formation of complexes or preferential binding would manifest itself as a very high R_1 of a particular fluorine atom compared to its neighbors. The oxygen molecule may prefer to approach the ends of the PFCs simply because there is more space available at the ends than in the bridgehead positions or the middle of a chain. This is clearly seen by comparing the slopes of different fluorine atoms of the cis and trans isomers of perfluorodecalin (PFD) (94). In the case of trans-perfluorodecalin, the larger difference in oxygen access to the end chain fluorine atoms compared to bridgehead fluorine atoms leads to a larger variability in the slopes compared to cis-perfluorodecalin. The slope does not vary greatly between terminal CF_3 groups of perfluorotributylamine (PFTB), perfluorotripropylamine (PFTP) and perfluorooctyl bromide (PFOB or perflubron) (91), and thus, relative pO_2 sensitivity of this resonance is determined by R_{1d}, which is different in all three cases. The CF_2 resonances from these PFCs show high sensitivity to temperature within the temperature range 5-50 °C. The terminal trifluoromethyl groups have greater sensitivity to oxygen and lower sensitivity to temperature (compared to CF_2 groups). The CF_3 resonance of PFOB exhibits greater sensitivity to pO_2 than PFTB or PFTP. Internal motion also aids R_{1p}, and hence pO_2 sensitivity. For example, the bulky CF_2Br group of PFOB is less sensitive to pO_2 than the CF_3 group on the other end of the molecule.

In general, each contribution (R_{1d} and R_{1p}) to R_1 is temperature dependent at a given field and exhibits a maximum at a temperature at which the inverse of corresponding correlation time matches the Larmor frequency. The constant k, which represents the oxygen solubility of the PFC, is also temperature dependent. On increasing the temperature, oxygen solubility in the PFC decreases and both R_{1p} and R_{1d} decrease for liquids in the motional narrowing regime ($\omega_0\tau_c << 1$). The temperature dependence of these relaxation rates can reveal information of the molecular dynamics that dominate these relaxation processes. In case of both anoxic and oxic PFTB the R_1 maxima were observed to occur at similar temperatures (91). This implies that in this case the τ_c that

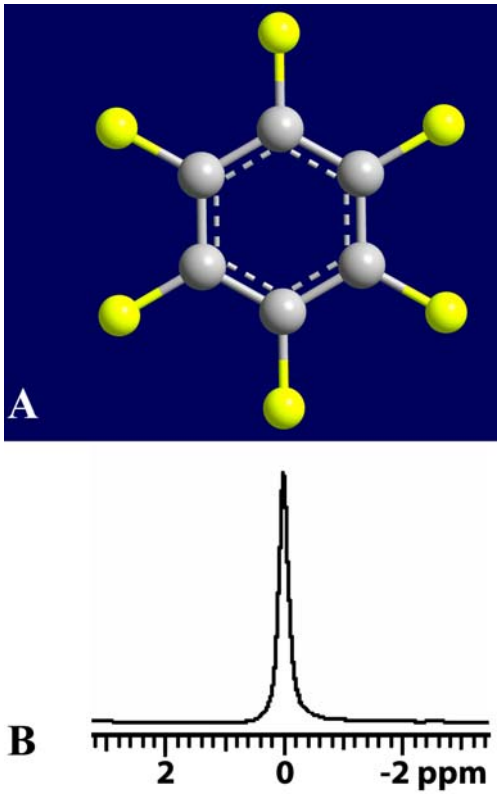

Figure 1. (a) Hexafluorobenzene and (b) its ^{19}F NMR spectrum.

determine R_{1p} and R_{1d} are approximately equal. Therefore, the residence time of an oxygen molecule near a given PFTB molecule may be comparable to the molecular rotational correlation time of PFTB. This represents a strong influence of residence time on R_{1p}, possibly as important as the inter-nuclear fluorine-oxygen distance.

3.4. Measuring pO_2

Although there is no theoretical reason to expect linearity in R_{1d} and R_{1p} with temperature, a linear approximation can be made for R_{1d} and R_{1p}/k from a purely practical standpoint within the biologically relevant temperature range (*e.g.*, 30-42 ^{o}C). If the respective relaxation rate maxima occur in the middle of this range, the slope and intercept may "appear" to be temperature independent). For characterizing the pO_2 and temperature dependence, the neat PFC or emulsion is typically placed in gas-tight NMR glass tubes, saturated by bubbling for 20-30 minutes with a range of standard gases (*e.g.*, 0%, 5%, 10%, 21% and 100 % O_2 -balance N_2) and sealed. Each sealed tube is inserted in a circulating water bath and the T_1 is measured as a function of temperature. The data at each temperature is fit to eqn. 3

$$R_1\,[s^{-1}] = A' + B' * pO_2 \quad (12)$$

where A' (=R_{1d}) and B' (=R_{1p}/k) are constants at a given temperature. If we assume a linear dependence of A' and B' on temperature T, then A'= A+C*T and B'= B+D*T, giving a temperature-dependent model (95):

$$R_1\,[s^{-1}] = A + B * pO_2 + C * T + D * pO_2 * T \quad (13)$$

where A, B, C and D are constants. For PFCs with multiple resonances theses constants are usually different for each resonance, discussed earlier. For such PFCs pO_2 and temperature can be estimated simultaneously by solving two simultaneous equations (corresponding to eqn. 13 for 2 resonances) using the measured values of R_1 for each resonance (95). In graphical terms, in a 3-dimensional variable space (R_1= f(pO_2, T)) the ordinates corresponding to the intersection of R_1 iso-contours of the two resonances are pO_2 and T, respectively. Multi resonance PFC spectra can provide multiple estimates of pO_2, if temperature is known, or pO_2 and temperature by solving simultaneous equations, as needed.

For imaging, multiple resonances could lead to chemical shift artifacts or reduced signal-to-noise following selective excitation or editing (96, 97). In practice, a PFC such as hexafluorobenzene (HFB) with a single resonance (Figure 1 a, b), high pO_2 sensitivity and minimal temperature sensitivity is preferable (75). Perfluoro-15-crown-5-ether (15-C-5) also has quite similar characteristics, and shorter absolute T_1s making data acquisition potentially faster, but a higher R_1 sensitivity to temperature and it is less readily available (9, 74). While a smaller A' value represents greater sensitivity, it also implies that the PFC has longer T_1 values (smaller R_1) under hypoxic conditions, where R_1 may be close to A'. Indeed, the T_1 of HFB at 4.7 T may reach 12 s, limiting the current temporal resolution of pO_2 measurements using HFB to 6 ½ min (98). However, use of echo planar imaging as in the *FREDOM* (Fluorocarbon Relaxometry using Echo planar imaging for Dynamic Oxygen Mapping) approach allows images, and hence, spatially resolved oxygen distributions to be acquired in the same time as spectroscopy (9). Following a direct intra-tissue injection, dynamic changes in oxygenation in response to hyperoxic intervention can be monitored *in vivo* (Figure 2). A further improvement in temporal resolution is possible by using other approaches such as those based on the Look-Locker technique (99, 100). Even then, a complete sampling of the relaxation curve would require at least 1 min (~ 5*T_1 for HFB under hypoxic conditions). The slope B' represents the effect of oxygen and hence a greater slope is desirable for measurement accuracy. A greater slope would result in a wider separation of measured T_1 values especially at low pO_2 values. A high slope could result from higher R_{1p} or a smaller k (higher O_2 solubility). From eqn. 2 we can see that for a given pO_2, a smaller k reflects a larger O_2 mole fraction x.

The solubility of oxygen (and gases in general) in perfluorocarbons and hydrofluorocarbons is three to ten times higher than observed in the parent hydrocarbons or in water (101, 102). It was shown that a model of continuous diffusion of oxygen, that accounts for the T_1 and T_2 relaxation of benzene, fails in the case of HFB, leading to either impossibly short residence times for oxygen or

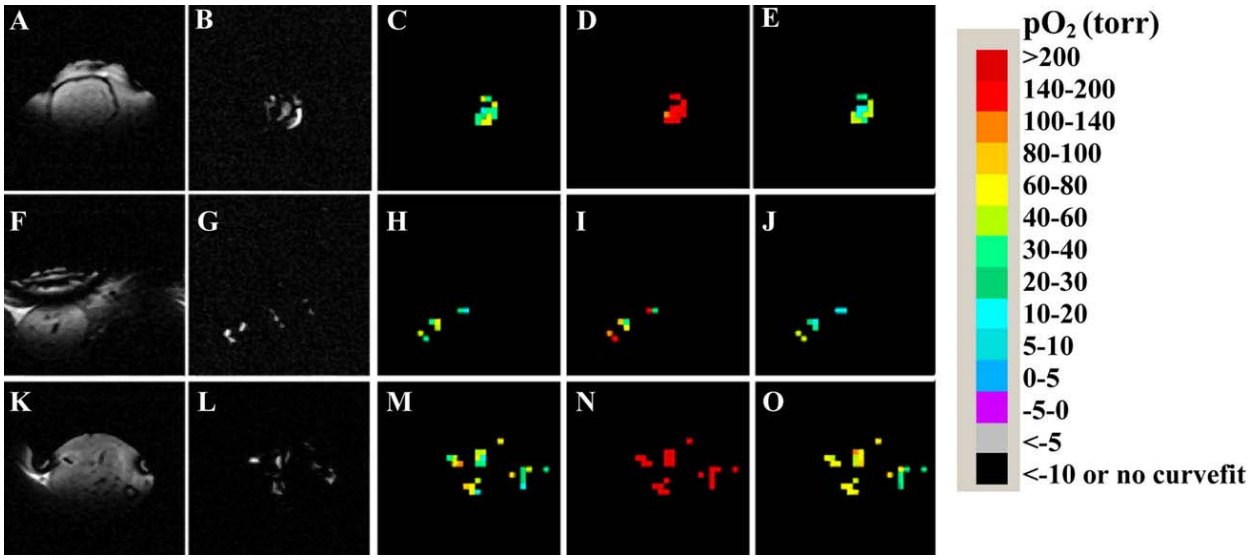

Figure 2. Dynamic ^{19}F MR oximetry. Monitoring changes in oxygenation at locations in the brain (a-e), kidney and liver (f-j) and thigh (k-o) of Sprague Dawley rat with respect to oxygen challenge following direct intra-tissue injection of HFB (50 µl) at discrete locations. Spin-echo anatomical images (a,f,k), spin-echo images of hexafluorobenzene injected into the tissue (b,g,l) and the corresponding time course *FREDOM* pO_2 maps (c,h,m: baseline air breathing, d,i,n: 30 min oxygen and e,j,o: 30 min after return to air breathing) showing the response to hyperoxic gas intervention. Data obtained in collaboration with Dr. Mark Rollins and Dr. Lisa Wilmes of UCSF.

impossibly small distance of closest approach between fluorine and oxygen (93). The presence of the larger fluorine atoms appears to result in the existence of numerous large "vacancies" or "channels" in the liquid "lattice", which the oxygen molecules occupy successively by random jumps. The oxygen solubility of long chained aliphatic fluorocarbons are observed to be higher than that of cyclic or aromatic fluorocarbons (102), which suggests that aliphatic chains form large channels in the liquid state, which accommodate more oxygen molecules unlike planar aromatic structures that may result in tighter "packing" with smaller vacancies. This exceptionally high solubility motivated the use of perfluorocarbons as blood substitutes for oxygen delivery to tissues (103, 104). Fluosol-DA (Green Cross Corp., Osaka, Japan) a perfluorotripropylamine based emulsion was the first PFC emulsion clinically tested and approved for clinical use as perfusate for percutaneous coronary angioplasty, but was later withdrawn from the market because of low oxygen delivery capacity under physiologic conditions, lack of clear clinical benefit and development of flow-through catheters (105-108). More recently, Oxygent^{TM} (Alliance Corp., San Diego, CA), an emulsion of perfluorooctyl bromide (perflubron) with a higher oxygen solubility and improved emulsion stability has been tested in clinical trials (109, 110). In terms of *in vivo* oximetry, due to their high oxygen solubility and hydrophobicity, PFCs essentially act as molecular amplifiers by displaying extra sensitivity to oxygen and insensitivity to variations in ionic constituents compared to the surrounding tissue water.

^{19}F MR based oximetry has several strengths and a few weaknesses. The nuclear spin ½ ^{19}F nucleus has γ of 40.05 MHz/T (compared to 42.58 MHz/T for ^{1}H) and about 83% NMR sensitivity compared to ^{1}H. It is 100 % abundant (isotopically) and the amount of endogenous fluorine in the body is very small (mostly present in form of solid fluorides in bones and teeth). Due to a very short T_2 relaxation time, the NMR signal from endogenous fluorine is undetectable in most biological systems. Given the absence of background signals, the exogenously administered PFC is readily observed. ^{19}F MR oximetry has been used as a research tool for many years (9, 74, 75, 84, 85, 98, 111-136). However, to date the method has not been translated to the routine clinical setting, since most clinical MRI scanners lack a ^{19}F capability. PFCs have been observed in patients following administration as adjuvant to radiotherapy and as residues in the eye, where they are used as tamponades during retinal surgery (127, 137, 138). A ^{1}H pO_2 reporter molecule could have greater immediate applicability and higher potential for clinical translation.

3.5. New development: ^{1}H MRI based oximetry using hexamethyldisiloxane

The ^{1}H R_1 of tissue water has been shown to be sensitive to tissue oxygenation (139), but many other factors like metal ions, cellularity, pH, ionic strength can also affect relaxation of tissue water. This makes quantitative measurements impossible except in tissues such as the vitreous humor in the eye and cerebrospinal fluid, where ionic and protein content is low or known and constant (140-143). Even then, R_1 sensitivity to oxygen is low (B'= 0.0002 s^{-1}/torr) and to temperature is high. We have recently identified hexamethyldisiloxane (HMDSO, Figure 3) as a ^{1}H NMR probe of pO_2 (analogous to PFCs) and shown the feasibility of tissue oximetry using ^{1}H-NMR spectroscopic relaxometry (83). We have also implemented

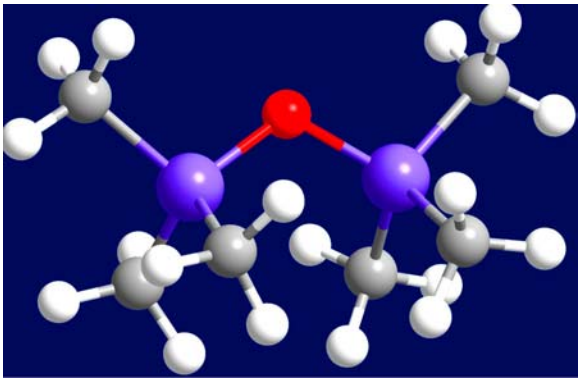

Figure 3. Structure of hexamethyldisiloxane (HMDSO).

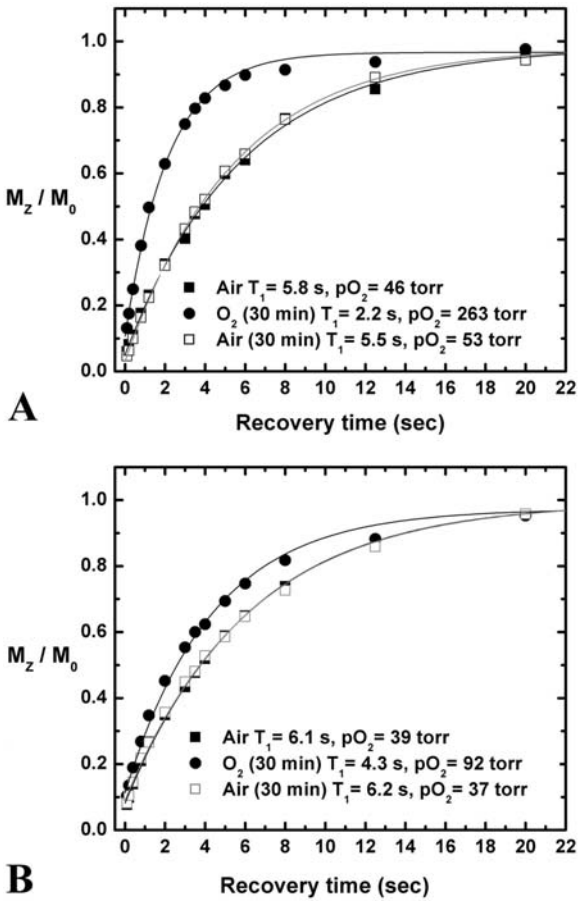

Figure 4. Dynamic ^{1}H oximetry. HMDSO magnetization recovery curves *in vivo* in response to hyperoxic challenge following direct intra-tissue injection of HMDSO (50 µl) at discrete locations. Chemical shift selective spectroscopy with suppression of fat and water signals permitted relaxometry of HMDSO. On switching breathing gas from air (■) to oxygen for 30 min (●) a larger change in T_1 (corresponding to a larger change in pO_2) is observed in thigh muscle **(a)** compared to AT1 prostate tumor **(b)** which is reversed in both cases by switching back to air breathing (□).

an imaging based method: Proton Imaging of Silanes to map Tissue Oxygenation Levels (*PISTOL*) for spatial mapping of pO_2 (144).

HMDSO is a symmetric molecule with a single NMR signal close to that of the chemical shift standard tetramethylsilane (TMS) (83). It is therefore well separated from water and reasonably separated from fat. HMDSO has many characteristics similar to PFCs: it is a highly hydrophobic mobile liquid, non-toxic, with high gas solubility and is readily available and cheap. At a given temperature, R_1 of HMDSO showed a linear dependence on pO_2, with constants A'= 0.1126 ± 0.0010[s^{-1}] and B'= 0.00130 ± 0.00002 [(torr*s)$^{-1}$] at 37 ^{o}C. The T_1 values range from 8.7 s (pO_2= 0 torr) to 1 s (pO_2= 760 torr) at 37 ^{o}C. A small temperature dependence was observed in the temperature range 26-46 ^{o}C. Fitting the calibration data to the temperature–dependant model (eqn. 13) yielded constants A = 0.1479 ± 0.0028 s^{-1}, B = (1.79 ± 0.05) X 10^{-3} (s torr)$^{-1}$, C = (-9.57 ± 0.81) X 10^{-4} (s ^{o}C)$^{-1}$, and D = (-1.23 ± 0.13) X 10^{-5} (s torr ^{o}C)$^{-1}$. In this temperature range, linear approximation resulted in errors < 3%. The pO_2 and temperature sensitivities of HMDSO are similar to 15-C-5.

Using a spectroscopic approach, pO_2 was measured in rat thigh muscle and Dunning prostate R3327 AT1 adenocarcinomas in response to an oxygen challenge (83). Changes in relaxation times in response to hyperoxia and differential response in tumor versus healthy thigh muscle can be easily seen from the HMDSO magnetization recovery curves (Figure 4). Clearance of HMDSO from muscle was seen to be slow with a half-life ~ 35 h, so that minimal change would be observed during typical MR studies of oxygen dynamics in response to acute interventions. HMDSO is quite inert and it has been reported that no treatment-related signs of toxicity or mortality or other statistically significant deleterious effects were noted in studies where Fisher rats were exposed to up to 6000 ppm HMDSO by inhalation (145, 146).

Like PFCs, HMDSO is lipophilic and is essentially immiscible in aqueous solutions. The boiling point and hydrophobicity of HMDSO suggest that it could be emulsified for intravenous delivery, as popular for several PFCs (147) and such an attempt is currently underway. HMDSO is readily and cheaply available from many commercial vendors and easy to store. One key difference in this ^{1}H MR approach compared to ^{19}F oximetry is the need to effectively suppress water and fat signals and perform relaxometry on the silane signal. In PISTOL, we have developed an effective approach using a combination of frequency selective excitation of the silane resonance and CHESS (148) suppression of the water and fat resonances is used followed by EPI detection for measuring T_1 values (144). As with HFB, ARDVARC (*A*lternating *R*elaxation *D*elays with *V*ariable *A*cquisitions for *R*eduction of *C*learance effects) protocol (98) is used in conjunction with this sequence to obtain T_1 values.

4. PERSPECTIVE AND CONCLUSION

An important advantage of MR oximetry compared to hypoxia imaging using nuclear and optical imaging agents is that one can quantitatively measure tissue pO_2 as opposed to qualitatively labeling hypoxic regions. Thus issues such as hypoxia specificity, oxygen dependency of agent binding and clearance of unbound agents do not come into play and affect interpretation. Dynamic measurements with transient interventions such as hyperoxia (9) or acute effects of vascular targeting (149) are not possible with nuclear and optical techniques. Optical imaging methods to image hypoxia to date rely on transfection to express bioluminescent (45, 47) or fluorescent proteins (44, 46) and are thus inappropriate for clinical application. In any case light penetration in tissue would be a problem for human use.

MR oximetry has found extensive use in pre clinical studies because it provides essentially unique insight into tissue oxygenation- specifically spatial and temporal resolution revealing heterogeneity and dynamic response to intervention. Moreover, precision achieved is appropriate for radiobiological studies of tumors. To date ^{19}F NMR approaches have been used to examine vascular oxygenation following i.v. administration of PFC emulsion or tissue oxygenation following vascular clearance and sequestration in tissue. However, accumulation occurs predominantly in tumor periphery biasing measurements towards well-perfused regions. Moreover, there is substantial uptake by the reticuloendothelial system (RES). While this allows effective measurements of pO_2 in liver, spleen and bone marrow, it is less satisfactory for oncological investigations. An alternate approach is direct injection of the reporter molecule into the tissue of interest. The possibility of targeting emulsion to specific antigens such fibrin for cardiovascular imaging opens further possibilities (150).

The development of PISTOL, a quantitative ^1H MR method for dynamic imaging of pO_2 opens further opportunities for *in vivo studies*. This method has a high potential of translation to the clinical setting. With current state-of-the-art MR hardware, it would be easy to generate effective water and fat suppression needed for PISTOL as used in detection of metabolites by Magnetic Resonance Spectroscopy (MRS). In both the research and clinical setting, it will now be possible to add quantitative oximetry to a protocol consisting of other ^1H-MR based functional techniques such as dynamic contrast enhancement, diffusion measurements, and MRS, but the minimal invasiveness of the technique has to be taken into account. Development of targeted nano-emulsions for intravenous delivery might help circumvent the need for direct intra-tissue injections, if high targeting specificity is achieved. Other ^1H pO_2 reporter molecules could be identified or synthesized, which could have higher oxygen sensitivity than HMDSO. We foresee MR oximetry as a valuable tool for assessing tissue oxygenation status in various disease states, helping to evaluate the acute and chronic response of therapeutic interventions and aiding in the screening of new drugs, such as vascular targeting and anti angiogenic agents which can perturb tissue oxygenation.

5. ACKNOWLEDGMENTS

Investigations discussed here have been supported by the Texas Affiliate of the American Heart Association, the Whitaker Foundation, the American Cancer Society, the Department of Defense Breast and Prostate Cancer Initiatives and the National Institute of Health. Most recent funding is from the NCI SAIRP U24 CA126608 and the work in Figure 2 was supported by the Foundation for Anesthesia Education and Research.

6. REFERENCES

1. Tatum, J. L., G. J. Kelloff, R. J. Gillies, J. M. Arbeit, J. M. Brown, K. S. Chao, J. D. Chapman, W. C. Eckelman, A. W. Fyles, A. J. Giaccia, R. P. Hill, C. J. Koch, M. C. Krishna, K. A. Krohn, J. S. Lewis, R. P. Mason, G. Melillo, A. R. Padhani, G. Powis, J. G. Rajendran, R. Reba, S. P. Robinson, G. L. Semenza, H. M. Swartz, P. Vaupel, D. Yang, B. Croft, J. Hoffman, G. Liu, H. Stone & D. Sullivan: Hypoxia: importance in tumor biology, noninvasive measurement by imaging, and value of its measurement in the management of cancer therapy. *Int J Radiat Biol*, 82, 699-757 (2006)

2. Okunieff, P., B. Fenton & Y. Chen: Past, present, and future of oxygen in cancer research. *Adv Exp Med Biol*, 566, 213-22 (2005)

3. Poli, G., G. Leonarduzzi, F. Biasi & E. Chiarpotto: Oxidative stress and cell signalling. *Curr Med Chem*, 11, 1163-82 (2004)

4. Bergamini, C. M., S. Gambetti, A. Dondi & C. Cervellati: Oxygen, reactive oxygen species and tissue damage. *Curr Pharm Des*, 10, 1611-26 (2004)

5. Brizel, D. M., G. S. Sibly, L. R. Prosmitz, R. L. Scher & M. W. Dewhirst: Tumor hypoxia adversely affects the prognosis of carcinoma of the head and neck. *Int. J. Radiat. Oncol. Biol. Phys.*, 38, 285-289 (1997)

6. Rofstad, E. K., K. Sundfor, H. Lyng & C. G. Trope: Hypoxia-induced treatment failure in advanced squamous cell carcinoma of the uterine cervix is primarily due to hypoxia-induced radiation resistance rather than hypoxia-induced metastasis. *Br. J. Cancer*, 83, 354-9 (2000)

7. Fyles, A., M. Milosevic, D. Hedley, M. Pintilie, W. Levin, L. Manchul & R. P. Hill: Tumor hypoxia has independent predictor impact only in patients with node-negative cervix cancer. *J Clin Oncol*, 20, 680-7 (2002)

8. Fyles, A., M. Milosevic, M. Pintilie, A. Syed, W. Levin, L. Manchul & R. P. Hill: Long-term performance of interstial fluid pressure and hypoxia as prognostic factors in cervix cancer. *Radiother Oncol*, 80, 132-7 (2006)

9. Zhao, D., L. Jiang & R. P. Mason: Measuring changes in tumor oxygenation. *Methods Enzymol*, 386, 378-418 (2004)

10. Swartz, H. M. & J. F. Dunn: Measurements of oxygen in tissues: overview and perspectives on methods. In: Oxygen Transport to Tissue XXIV. Eds: J. F. Dunn&H. M. Swartz. Kluwer Academic, New York (2003)

11. Stone, H. B., J. M. Brown, T. Phillips & R. M. Sutherland: Oxygen in human tumors: correlations between

methods of measurement and response to therapy. *Radiat. Res.*, 136, 422-434 (1993)
12. Vaupel, P., K. Schlenger, C. Knoop & M. Hockel: Oxygenation of human tumors: evaluation of tissue oxygen distribution in breast cancers by computerized O_2 tension measurements. *Cancer Res*, 51, 3316-22 (1991)
13. Cater, D. B. & I. A. Silver: Quantitative measurements of oxygen tension in normal tissues and in the tumours of patients before and after radiotherapy. *Acta radiol*, 53, 233-56 (1960)
14. Crawford, D. W. & M. A. Cole: Performance evaluation of recessed microcathodes: criteria for tissue pO_2 measurement. *J Appl Physiol*, 58, 1400-5 (1985)
15. Nozue, M., I. Lee, F. Yuan, B. A. Teicher, D. M. Brizel, M. W. Dewhirst, C. G. Milross, L. Milas, C. W. Song, C. D. Thomas, M. Guichard, S. M. Evans, C. J. Koch, E. M. Lord, R. K. Jain & H. D. Suit: Interlaboratory variation in oxygen tension measurement by Eppendorf "Histograph" and comparison with hypoxic marker. *J Surg Oncol*, 66, 30-8 (1997)
16. Brizel, D. M., S. P. Scully, J. M. Harrelson, L. J. Layfield, J. M. Bean, L. R. Prosnitz & M. W. Dewhirst: Tumor oxygenation predicts for the likelihood of distant metastases in human soft tissue sarcoma. *Cancer Res.*, 56, 941-3 (1996)
17. Movsas, B., J. D. Chapman, E. M. Horwitz, W. H. Pinover, R. E. Greenberg, A. L. Hanlon, R. Iyer & G. E. Hanks: Hypoxic regions exist in human prostate carcinoma. *Urology*, 53, 11-8 (1999)
18. Rudat, V., B. Vanselow, P. Wollensack, C. Bettscheider, S. Osman-Ahmet, M. J. Eble & A. Dietz: Repeatability and prognostic impact of the pretreatment pO_2 histography in patients with advanced head and neck cancer. *Radiother Oncol*, 57, 31-7 (2000)
19. Aquino-Parsons, C., A. Green & A. I. Minchinton: Oxygen tension in primary gynaecological tumours: the influence of carbon dioxide concentration. *Radiother Oncol*, 57, 45-51 (2000)
20. Griffiths, J. R. & S. P. Robinson: The OxyLite: a fibre-optic oxygen sensor. *British Journal of Radiology*, 72, 627-630 (1999)
21. Bussink, J., J. H. A. M. Kaanders, A. M. Strik, B. Vojnovic & A. J. van der Kogel: Optical sensor-based oxygen tension measurements correspond with hypoxia marker binding in three human tumor xenograft lines. *Radiation Research*, 154, 547-555 (2000)
22. Mason, R. P., D. Zhao, A. Constantinescu & A. Obeid: Tumor oximetry: comparison of ^{19}F MR EPI (FREDOM) and the fiber-optic OxyLite™. *Proc Intl Soc Magn Reson Med*, 8, 1040 (2000)
23. Braun, R. D., J. L. Lanzen, S. A. Snyder & M. W. Dewhirst: Comparison of tumor and normal tissue oxygen tension measurements using OxyLite or microelectrodes in rodents. *Am J Physiol Heart Circ Physiol*, 280, H2533-44 (2001)
24. Seddon, B. M., D. J. Honess, B. Vojnovic, G. M. Tozer & P. Workman: Measurement of tumor oxygenation: *in vivo* comparison of a luminescence fiber-optic sensor and a polarographic electrode in the p22 tumor. *Radiat Res*, 155, 837-46 (2001)
25. Jarm, T., G. Sersa & D. Miklavcic: Oxygenation and blood flow in tumors treated with hydralazine: evaluation with a novel luminescence-based fiber-optic sensor. *Technol Health Care*, 10, 363-80 (2002)
26. Urano, M., Y. Chen, J. Humm, J. A. Koutcher, P. Zanzonico & C. Ling: Measurements of tumor tissue oxygen tension using a time-resolved luminescence-based optical oxylite probe: comparison with a paired survival assay. *Radiat Res*, 158, 167-73 (2002)
27. Gu, Y. Q., V. A. Bourke, J. G. Kim, A. Constantinescu, R. P. Mason & H. L. Liu: Dynamic response of breast tumor oxygenation to hyperoxic respiratory challenge monitored with three oxygen-sensitive parameters. *Applied Optics*, 42, 2960-2967 (2003)
28. Brurberg, K. G., H. K. Skogmo, B. A. Graff, D. R. Olsen & E. K. Rofstad: Fluctuations in pO_2 in poorly and well-oxygenated spontaneous canine tumors before and during fractionated radiation therapy. *Radiother Oncol*, 77, 220-6 (2005)
29. Brurberg, K. G., M. Thuen, E. B. Ruud & E. K. Rofstad: Fluctuations in pO_2 in irradiated human melanoma xenografts. *Radiat Res*, 165, 16-25 (2006)
30. Elas, M., K. H. Ahn, A. Parasca, E. D. Barth, D. Lee, C. Haney & H. J. Halpern: Electron paramagnetic resonance oxygen images correlate spatially and quantitatively with Oxylite oxygen measurements. *Clin Cancer Res*, 12, 4209-17 (2006)
31. Wen, B., M. Urano, J. A. O'Donoghue & C. C. Ling: Measurements of partial oxygen pressure pO_2 using the OxyLite system in R3327-AT tumors under isoflurane anesthesia. *Radiat Res*, 166, 512-8 (2006)
32. Ballinger, J. R.: Imaging hypoxia in tumors. *Semin Nucl Med*, 31, 321-9 (2001)
33. Ljungkvist, A. S., J. Bussink, J. H. Kaanders & A. J. van der Kogel: Dynamics of tumor hypoxia measured with bioreductive hypoxic cell markers. *Radiat Res*, 167, 127-45 (2007)
34. Maxwell, R. J., P. Workman & J. R. Griffiths: Demonstration of tumor-selective retention of fluorinated nitroimidazole probes by ^{19}F magnetic resonance spectroscopy *in vivo*. *Int J Radiat Oncol Biol Phys*, 16, 925-9 (1989)
35. Raleigh, J. A., A. J. Franko, D. A. Kelly, L. A. Trimble & P. S. Allen: Development of an *in vivo* ^{19}F magnetic resonance method for measuring oxygen deficiency in tumors. *Magn Reson Med*, 22, 451-66 (1991)
36. Aboagye, E. O., R. J. Maxwell, M. R. Horsman, A. D. Lewis, P. Workman, M. Tracy & J. R. Griffiths: The relationship between tumour oxygenation determined by oxygen electrode measurements and magnetic resonance spectroscopy of the fluorinated 2-nitroimidazole SR-4554. *Br J Cancer*, 77, 65-70 (1998)
37. Jerabek, P. A., T. B. Patrick, M. R. Kilbourn, D. D. Dischino & M. J. Welch: Synthesis and biodistribution of ^{18}F-labeled fluoronitroimidazoles: potential *in vivo* markers of hypoxic tissue. *Int J Rad Appl Instrum [A]*, 37, 599-605 (1986)
38. Rasey, J. S., Z. Grunbaum, S. Magee, N. J. Nelson, P. L. Olive, R. E. Durand & K. A. Krohn: Characterization of radiolabeled fluoromisonidazole as a probe for hypoxic cells. *Radiat Res*, 111, 292-304 (1987)
39. Lewis, J. S., D. W. McCarthy, T. J. McCarthy, Y. Fujibayashi & M. J. Welch: Evaluation of 64Cu-ATSM *in*

vitro and *in vivo* in a hypoxic tumor model. *J Nucl Med*, 40, 177-83 (1999)
40. Dolbier, W. R., Jr., A. R. Li, C. J. Koch, C. Y. Shiue & A. V. Kachur: [18F]-EF5, a marker for PET detection of hypoxia: synthesis of precursor and a new fluorination procedure. *Appl Radiat Isot*, 54, 73-80 (2001)
41. Mannan, R. H., V. V. Somayaji, J. Lee, J. R. Mercer, J. D. Chapman & L. I. Wiebe: Radioiodinated 1- (5-iodo-5-deoxy-beta-D-arabinofuranosyl)-2-nitroimidazole (iodoazomycin arabinoside: IAZA): a novel marker of tissue hypoxia. *J Nucl Med*, 32, 1764-70 (1991)
42. Li, L., J. M. Yu, L. G. Xing, G. R. Yang, X. D. Sun, J. Xu, H. Zhu & J. B. Yue: Hypoxic imaging with 99mTc-HL91 single photon emission computed tomography in advanced nonsmall cell lung cancer. *Chin Med J (Engl)*, 119, 1477-80 (2006)
43. Takahashi, E., T. Takano, Y. Nomura, S. Okano, O. Nakajima & M. Sato: *In vivo* oxygen imaging using green fluorescent protein. *Am J Physiol Cell Physiol*, 291, C781-7 (2006)
44. Vordermark, D., T. Shibata & J. M. Brown: Green fluorescent protein is a suitable reporter of tumor hypoxia despite an oxygen requirement for chromophore formation. *Neoplasia*, 3, 527-34 (2001)
45. Payen, E., M. Bettan, A. Henri, E. Tomkiewitcz, A. Houque, I. Kuzniak, J. Zuber, D. Scherman & Y. Beuzard: Oxygen tension and a pharmacological switch in the regulation of transgene expression for gene therapy. *J Gene Med*, 3, 498-504 (2001)
46. Raman, V., D. Artemov, A. P. Pathak, P. T. Winnard, Jr., S. McNutt, A. Yudina, A. Bogdanov, Jr. & Z. M. Bhujwalla: Characterizing vascular parameters in hypoxic regions: a combined magnetic resonance and optical imaging study of a human prostate cancer model. *Cancer Res*, 66, 9929-36 (2006)
47. Safran, M., W. Y. Kim, F. O'Connell, L. Flippin, V. Gunzler, J. W. Horner, R. A. Depinho & W. G. Kaelin, Jr.: Mouse model for noninvasive imaging of HIF prolyl hydroxylase activity: assessment of an oral agent that stimulates erythropoietin production. *Proc Natl Acad Sci U S A*, 103, 105-10 (2006)
48. Abramovitch, R., D. Frenkiel & M. Neeman: Analysis of subcutaneous angiogenesis by gradient echo magnetic resonance imaging. *Magn. Reson. Med.*, 39, 813-24 (1998)
49. Brasch, R. C., K. C. Li, J. E. Husband, M. T. Keogan, M. Neeman, A. R. Padhani, D. Shames & K. Turetschek: *In vivo* monitoring of tumor angiogenesis with MR imaging. [Review]. *Acad. Radiol.*, 7, 812-23 (2000)
50. Cao, Y., Z. Shen, T. L. Chenevert & J. R. Ewing: Estimate of vascular permeability and cerebral blood volume using Gd-DTPA contrast enhancement and dynamic T2*-weighted MRI. *J Magn Reson Imaging*, 24, 288-96 (2006)
51. Roberts, T. P. & H. A. Rowley: Diffusion weighted magnetic resonance imaging in stroke. *Eur J Radiol*, 45, 185-94 (2003)
52. Sotak, C. H.: Nuclear magnetic resonance (NMR) measurement of the apparent diffusion coefficient (ADC) of tissue water and its relationship to cell volume changes in pathological states. *Neurochem Int*, 45, 569-82 (2004)
53. Sykova, E.: Diffusion properties of the brain in health and disease. *Neurochem Int*, 45, 453-66 (2004)
54. Charles-Edwards, E. M. & N. M. deSouza: Diffusion-weighted magnetic resonance imaging and its application to cancer. *Cancer Imaging*, 6, 135-43 (2006)
55. Foltz, W. D., N. Merchant, E. Downar, J. A. Stainsby & G. A. Wright: Coronary venous oximetry using MRI. *Magnetic Resonance in Medicine*, 42, 837-48 (1999)
56. Neeman, M., H. Dafni, O. Bukhari, R. D. Braun & M. W. Dewhirst: *In vivo* BOLD contrast MRI mapping of subcutaneous vascular function and maturation: validation by intravital microscopy. *Magn. Reson. Med.*, 45, 887-98 (2001)
57. Howe, F. A., S. P. Robinson, D. J. McIntyre, M. Stubbs & J. R. Griffiths: Issues in flow and oxygenation dependent contrast (FLOOD) imaging of tumours. *NMR in Biomed.*, 14, 497-506 (2001)
58. Baudelet, C. & B. Gallez: How does blood oxygen level-dependent (BOLD) contrast correlate with oxygen partial pressure (pO_2) inside tumors? *Magn. Reson. Med.*, 48, 980-986 (2002)
59. Baudelet, C. & B. Gallez: Current issues in the utility of blood oxygen level dependent MRI for the assessment of modulations in tumor oxygenation *Curr Med Imaging Rev.*, 1, 229-243 (2005)
60. Bhujwalla, Z. M., D. Artemov, E. Aboagye, E. Ackerstaff, R. J. Gillies, K. Natarajan & M. Solaiyappan: The physiological environment in cancer vascularization, invasion and metastasis. *Novartis Found Symp*, 240, 23-38; discussion 38-45, 152-3 (2001)
61. Gillies, R. J., Z. M. Bhujwalla, J. Evelhoch, M. Garwood, M. Neeman, S. P. Robinson, C. H. Sotak & B. Van Der Sanden: Applications of magnetic resonance in model systems: tumor biology and physiology. *Neoplasia*, 2, 139-51 (2000)
62. Yu, J. X., V. Kodibagkar, W. Cui & R. P. Mason: ^{19}F: a versatile reporter for non-invasive physiology and pharmacology using magnetic resonance. *Curr. Med. Chem.*, 12, 818-848 (2005)
63. Evans, S. M., S. Hahn, D. R. Pook, W. T. Jenkins, A. A. Chalian, P. Zhang, C. Stevens, R. Weber, G. Weinstein, I. Benjamin, N. Mirza, M. Morgan, S. Rubin, W. G. McKenna, E. M. Lord & C. J. Koch: Detection of hypoxia in human squamous cell carcinoma by EF5 binding. *Cancer Res*, 60, 2018-24 (2000)
64. Aime, S., C. Cabella, S. Colombatto, S. Geninatti Crich, E. Gianolio & F. Maggioni: Insights into the use of paramagnetic Gd (III) complexes in MR-molecular imaging investigations. *JMRI*, 16, 394-406 (2002)
65. Kurhanewicz, J., D. B. Vigneron, R. G. Males, M. G. Swanson, K. K. Yu & H. Hricak: The prostate: MR imaging and spectroscopy. Present and future. [Review]. *Radiol. Clin. North Amer.*, 38, 115-38 (2000)
66. Minati, L., M. Grisoli & M. G. Bruzzone: MR spectroscopy, functional MRI, and diffusion-tensor imaging in the aging brain: a conceptual review. *J Geriatr Psychiatry Neurol*, 20, 3-21 (2007)
67. Cecil, K. M.: MR spectroscopy of metabolic disorders. *Neuroimaging Clin N Am*, 16, 87-116, viii (2006)
68. Horn, M.: Cardiac magnetic resonance spectroscopy: a window for studying physiology. *Methods Mol Med*, 124, 225-48 (2006)
69. Shah, N., A. Sattar, M. Benanti, S. Hollander & L. Cheuck: Magnetic resonance spectroscopy as an imaging

tool for cancer: a review of the literature. *J Am Osteopath Assoc*, 106, 23-7 (2006)
70. De Stefano, N. & M. Filippi: MR spectroscopy in multiple sclerosis. *J Neuroimaging*, 17 Suppl 1, 31S-35S (2007)
71. Martin, W. R.: MR Spectroscopy in Neurodegenerative Disease. *Mol Imaging Biol* (2007)
72. Li, K. C. P., G. A. Wright, L. R. Pelc, R. L. Dalamn, J. H. Brittain, H. Wegmueller, J. T. Lin & C. K. Song: Oxygen saturation of blood in the superior mesenteric vein. *Radiology*, 194, 321-325 (1995)
73. Wright, G. A., B. S. Hu & A. Macovski: Estimating oxygen saturation of blood *in vivo* with MR imaging at 1.5 T. *JMRI*, 1, 275-283 (1991)
74. Dardzinski, B. J. & C. H. Sotak: Rapid tissue oxygen tension mapping using ^{19}F inversion-recovery echo-planar imaging of perfluoro-15-crown-5-ether. *Magn Reson Med*, 32, 88-97 (1994)
75. Mason, R. P., W. Rodbumrung & P. P. Antich: Hexafluorobenzene: a sensitive ^{19}F NMR indicator of tumor oxygenation. *NMR Biomed.*, 9, 125-134 (1996)
76. Mason, R. P.: Non-invasive physiology: ^{19}F NMR of perfluorocarbons. *Artif Cells Blood Substit Immobil Biotechnol*, 22, 1141-53 (1994)
77. Glockner, J. F. & H. M. Swartz: *In vivo* EPR oximetry using two novel probes: fusinite and lithium phthalocyanine. *Adv Exp Med Biol*, 317, 229-34 (1992)
78. Swartz, H. M., K. J. Liu, F. Goda & T. Walczak: India ink: a potential clinically applicable EPR oximetry probe. *Magn. Reson. Med.*, 31, 229-232 (1994)
79. Zweier, J. L. & P. Kuppusamy: Electron paramagnetic resonance measurements of free radicals in the intact beating heart: A technique for detection and characterization of free radicals in whole biological tissues. *Proc. Natl. Acad. Sci. (USA)*, 85, 5703-5707 (1988)
80. Matsumoto, A., S. Matsumoto, A. L. Sowers, J. W. Koscielniak, N. J. Trigg, P. Kuppusamy, J. B. Mitchell, S. Subramanian, M. C. Krishna & K. Matsumoto: Absolute oxygen tension (pO_2) in murine fatty and muscle tissue as determined by EPR. *Magn Reson Med*, 54, 1530-5 (2005)
81. Gallez, B., C. Baudelet & B. F. Jordan: Assessment of tumor oxygenation by electron paramagnetic resonance: principles and applications. *NMR Biomed*, 17, 240-62 (2004)
82. Gallez, B. & H. M. Swartz: *In vivo* EPR: when, how and why? *NMR Biomed*, 17, 223-5 (2004)
83. Kodibagkar, V. D., W. Cui, M. E. Merritt & R. P. Mason: Novel 1H NMR approach to quantitative tissue oximetry using hexamethyldisiloxane. *Magn Reson Med*, 55, 743-8 (2006)
84. Thomas, S. R.: The biomedical applications of Fluorine-19 NMR. In: Magnetic Resonance Imaging. Eds: C. L. Partain, R. R. Price, J. A. Patton, M. V. Kulkarni&A. E. J. James. W.B. Saunders Co., London (1988)
85. Mason, R. P.: Non-invasive physiology: ^{19}F NMR of perfluorocarbon. *Art. Cells, Blood Sub. & Immob. Biotech.*, 22, 1141-1153 (1994)
86. Abragam, A.: The Principles of Nuclear Magnetism. Oxford University Press, New York (1961)
87. McConnell, H. M. & C. H. Holm: Anisotropic chemical shielding and nuclear magnetic relaxation in liquids. *J. Chem. Phys.*, 25, 1289 (1956)
88. Blicharski, J. S.: Interference effect in nuclear magnetic relaxation. *Phys. Lett. A*, 24, 608 (1967)
89. Farrar, T. C. & J. D. Decatur: Temperature-Dependent NMR Relaxation Studies of Na_2PHO_3 in Solution. *J Phys Chem*, 94, 7395-7401 (1990)
90. Matson, G. B.: Methyl NMR relaxation: the effects of spin rotation and chemical shift anisotropy mechanisms. *J. Chem. Phys.*, 67, 5152 (1977)
91. Shukla, H. P., R. P. Mason, D. E. Woessner & P. P. Antich: A comparison of three commercial perfluorocarbon emulsions as high field NMR probes of oxygen tension and temperature. *J. Magn. Reson. Series B*, 106, 131-141 (1995)
92. Hunjan, S., R. P. Mason, A. Constantinescu, P. Peschke, E. W. Hahn & P. P. Antich: Regional tumor oximetry: ^{19}F NMR spectroscopy of hexafluorobenzene. *Int J Radiat Oncol Biol Phys*, 41, 161-71 (1998)
93. Delpuech, J. J., M. A. Hamza, G. Serratrice & M. J. Stebe: Fluorocarbons as Oxygen Carriers .1. Nmr-Study of Oxygen Solutions in Hexafluorobenzene. *J Chem Phys*, 70, 2680-2687 (1979)
94. Parhami, P. & B. M. Fung: F-19 Relaxation Study of Perfluoro Chemicals as Oxygen Carriers. *J Phys Chem*, 87, 1928-1931 (1983)
95. Mason, R. P., H. Shukla & P. P. Antich: *In vivo* oxygen tension and temperature: simultaneous determination using ^{19}F NMR spectroscopy of perfluorocarbon. *Magn Reson Med*, 29, 296-302 (1993)
96. Mason, R. P., P. P. Antich, E. E. Babcock, J. L. Gerberich & R. L. Nunnally: Perfluorocarbon imaging *in vivo*: A ^{19}F MRI study in tumor-bearing mice. *Magn. Reson. Imaging*, 7, 475-485 (1989)
97. Babcock, E. E., R. P. Mason & P. P. Antich: Effect of homonuclear J modulation on ^{19}F spin-echo images. *Magn. Reson. Med.*, 17, 178-188 (1991)
98. Hunjan, S., D. Zhao, A. Constantinescu, E. W. Hahn, P. P. Antich & R. P. Mason: Tumor oximetry: demonstration of an enhanced dynamic mapping procedure using fluorine-19 echo planar magnetic resonance imaging in the Dunning prostate R3327-AT1 rat tumor. *Int J Radiat Oncol Biol Phys*, 49, 1097-108 (2001)
99. Look, D. C. & D. R. Locker: Time saving in measurement of NMR and EPR relaxation times. *Rev. Sci. Instrum.*, 41, 250 (1970)
100. Caruthers, S. D., P. J. Gaffney, F. D. Hockett, R. Lamerichs, G. M. Lanza, A. M. Neubauer, M. J. Scott, S. A. Wickline & P. M. Winter: 19F MR techniques augment quantitative molecular imaging with paramagnetic perfluorocarbon nanoparticles at 1.5 T. *Proc Intl Soc Magn Reson Med*, 14, 1834 (2006)
101. Hamza, M. A., G. Serratrice, M. J. Stebe & J. J. Delpuech: Fluorocarbons as Oxygen Carriers .2. An Nmr-Study of Partially or Totally Fluorinated Alkanes and Alkenes. *J Magn Reson*, 42, 227-241 (1981)
102. Hamza, M. A., G. Serratrice, M. J. Stebe & J. J. Delpuech: Solute-Solvent Interactions in Perfluorocarbon Solutions of Oxygen - an Nmr-Study. *JACS*, 103, 3733-3738 (1981)
103. Kim, H. W. & A. G. Greenburg: Artificial oxygen carriers as red blood cell substitutes: a selected review and current status. *Artif Organs*, 28, 813-28 (2004)

104. Riess, J. G.: Perfluorocarbon-based oxygen delivery. *Artif Cells Blood Substit Immobil Biotechnol*, 34, 567-80 (2006)
105. Tremper, K. K., G. M. Vercellotti & D. E. Hammerschmidt: Hemodynamic Profile of Adverse Clinical Reactions to Fluosol-Da 20-Percent. *Critical Care Medicine*, 12, 428-431 (1984)
106. Gould, S. A., A. L. Rosen, L. R. Sehgal, H. L. Sehgal, L. A. Langdale, L. M. Krause, C. L. Rice, W. H. Chamberlin & G. S. Moss: Fluosol-Da as a Red-Cell Substitute in Acute Anemia. *New England Journal of Medicine*, 314, 1653-1656 (1986)
107. Bell, M. R., R. A. Nishimura, D. R. Holmes, K. R. Bailey, R. S. Schwartz & R. E. Vlietstra: Does Intracoronary Infusion of Fluosol-Da 20-Percent Prevent Left-Ventricular Diastolic Dysfunction During Coronary Balloon Angioplasty. *J Am Coll Cardiol*, 16, 959-966 (1990)
108. Kent, K. M., M. W. Cleman, M. J. Cowley, M. B. Forman, C. C. Jaffe, M. Kaplan, S. B. King, M. W. Krucoff, T. Lassar, B. McAuley, R. Smith, C. Wisdom & D. Wohlgelernter: Reduction of Myocardial-Ischemia During Percutaneous Transluminal Coronary Angioplasty with Oxygenated Fluosol. *Am J Cardiol*, 66, 279-284 (1990)
109. Spahn, D. R., K. F. Waschke, T. Standl, J. Motsch, L. Van Huynegem, M. Welte, H. Gombotz, P. Coriat, L. Verkh, S. Faithfull & P. Keipert: Use of perflubron emulsion to decrease allogeneic blood transfusion in high-blood-loss non-cardiac surgery: results of a European phase 3 study. *Anesthesiology*, 97, 1338-49 (2002)
110. Hill, S. E., B. J. Leone, N. S. Faithfull, K. E. Flaim, P. E. Keipert & M. F. Newman: Perflubron emulsion (AF0144) augments harvesting of autologous blood: a phase II study in cardiac surgery. *J Cardiothorac Vasc Anesth*, 16, 555-60 (2002)
111. Thomas, S. R., R. W. Millard, R. G. Pratt, Y. Shiferaw & R. C. Samaratunga: Quantitative pO_2 imaging *in vivo* with perfluorocarbon F-19 NMR: tracking oxygen from the airway through the blood to organ tissues. *Art Cells, Blood Subst. Immob. Biotechnol.*, 22, 1029-1042 (1994)
112. Thomas, S. R., R. G. Pratt, R. W. Millard, R. C. Samaratunga, Y. Shiferaw, L. C. Clark Jr. & R. E. Hoffmann: Evaluation of the Influence of the Aqueous Phase Bioconstituent Environment on the F-19 T1 of Perfluorocarbon Blood Substitute Emulsions. *JMRI*, 4, 631-635 (1994)
113. Thomas, S. R., R. G. Pratt, R. W. Millard, R. C. Samaratunga, Y. Shiferaw, A. J. McGoron & K. K. Tan: *In vivo* pO_2 imaging in the porcine model with perfluorocarbon F-19 NMR at low field. *Magn. Reson. Imaging*, 14, 103-114 (1996)
114. Zhao, D., A. Constantinescu, C.-H. Chang, E. W. Hahn & R. P. Mason: Correlation of Tumor Oxygen Dynamics with Radiation Response of the Dunning Prostate R3327-HI Tumor. *Radiat. Res.*, 159, 621-631 (2003)
115. Zhao, D., A. Constantinescu, L. Jiang, E. W. Hahn & R. P. Mason: Prognostic Radiology: quantitative assessment of tumor oxygen dynamics by MRI. *Am. J. Clin. Oncol*, 24, 462-466 (2001)
116. Zhao, D., S. Ran, A. Constantinescu, E. W. Hahn & R. P. Mason: Tumor oxygen dynamics: correlation of *in vivo* MRI with histological findings. *Neoplasia*, 5, 308-18 (2003)
117. Mason, R. P., P. P. Antich, E. E. Babcock, A. Constantinescu, P. Peschke & E. W. Hahn: Non-invasive determination of tumor oxygen tension and local variation with growth. *Int. J. Radiat. Oncol. Biol. Phys.*, 29, 95-103 (1994)
118. Mason, R. P., F. M. H. Jeffrey, C. R. Malloy, E. E. Babcock & P. P. Antich: A noninvasive assessment of myocardial oxygen tension: ^{19}F NMR spectroscopy of sequestered perfluorocarbon emulsion. *Magn. Reson. Med.*, 27, 310-317 (1992)
119. Mason, R. P., H. P. Shukla & P. P. Antich: Oxygent: a novel probe of tissue oxygen tension. *Biomater. Artif. Cells Immob. Biotechnol.*, 20, 929-935 (1992)
120. Hunjan, S., R. P. Mason, A. Constantinescu, P. Peschke, E. W. Hahn & P. P. Antich: Regional tumor oximetry: ^{19}F NMR spectroscopy of hexafluorobenzene. *Int. J. Radiat. Oncol. Biol. Phys.*, 40, 161-71 (1998)
121. Song, Y., A. Constantinescu & R. P. Mason: Dynamic Breast tumor oximetry: the development of Prognostic Radiology. *Technol. Cancer Res. Treat.*, 1, 471-478 (2002)
122. Xia, M., V. Kodibagkar, H. Liu & R. P. Mason: Tumour oxygen dynamics measured simultaneously by near infrared spectroscopy and ^{19}F magnetic resonance imaging in rats. *Phys. Med. Biol.*, 51, 45-60 (2006)
123. Barker, B. R., R. P. Mason, N. Bansal & R. M. Peshock: Oxygen tension mapping by ^{19}F echo planar NMR imaging of sequestered perfluorocarbon. *JMRI*, 4, 595-602 (1994)
124. Sotak, C. H., P. S. Hees, H.-H. Huang, M.-H. Hung, C. G. Krespan & S. Reynolds: A new perfluorocarbon for use in fluorine-19 magnetic resonance spectroscopy. *Magn. Reson. Med.*, 29, 188-195 (1993)
125. Sotak, C. H., P. S. Hees, H. N. Huang, M. H. Hung, C. G. Krespan & S. Raynolds: A new perfluorocarbon for use in fluorine-19 MRI and MRS. *Magn. Reson. Med*, 29, 188-95 (1993)
126. Berkowitz, B. A., C. A. Wilson, D. L. Hatchell & R. E. London: Quantitative determination of the partial oxygen pressure in the vitrectomized rabbit eye *in vivo* using ^{19}F NMR. *Magn Reson Med*, 21, 233-41 (1991)
127. Wilson, C., B. Berkowitz, B. McCuen & C. Charles: Measurement of preretinal pO2 in the vitrectomized human eye using ^{19}F NMR. *Arch. Ophthalmol*, 110, 1098-100 (1992)
128. Noth, U., S. P. Morrissey, R. Deichmann, H. Adolf, C. Schwarzbauer, J. Lutz & A. Haase: *In vivo* measurement of partial oxygen pressure in large vessels and in the reticuloendothelial system using fast ^{19}F-MRI. *Magn Reson Med*, 34, 738-45 (1995)
129. Noth, U., P. Grohn, A. Jork, U. Zimmermann, A. Haase & J. Lutz: ^{19}F-MRI *in vivo* determination of the partial oxygen pressure in perfluorocarbon-loaded alginate capsules implanted into the peritoneal cavity and different tissues. *Magn Reson Med*, 42, 1039-47 (1999)
130. Mattrey, R. F., D. J. Schumacher, H. T. Tran, Q. Guo & R. B. Buxton: The use of Imagent BP in diagnostic imaging research and ^{19}F magnetic resonance for PO2

measurements. *Biomaterials, Artificial Cells, & Immobilization Biotechnology.*, 20, 917-20 (1992)
131. McIntyre, D. J. O., C. L. McCoy & J. R. Griffiths: Tumour oxygenation measurements by ^{19}F MRI of perfluorocarbons. *Curr. Sci.*, *76*, 753-762 (1999)
132. Bellemann, M. E., J. Bruckner, P. Peschke, G. Brix & R. P. Mason: [Quantification and visualization of oxygen partial pressure *in vivo* by 19F NMR imaging of perfluorocarbons]. *Biomed Tech (Berl)*, 47 Suppl 1 Pt 1, 451-4 (2002)
133. Lutz, J., U. Noth, S. P. Morrissey, H. Adolf, R. Deichmann & A. Haase: Measurement of oxygen tensions in the abdominal cavity and in the skeletal muscle using ^{19}F-MRI of neat PFC droplets. *Adv Exp Med Biol*, 428, 569-72 (1997)
134. Zimmermann, U., U. Noth, P. Grohn, A. Jork, K. Ulrichs, J. Lutz & A. Haase: Non-invasive evaluation of the location, the functional integrity and the oxygen supply of implants: 19F nuclear magnetic resonance imaging of perfluorocarbon-loaded Ba2+-alginate beads. *Artif Cells Blood Substit Immobil Biotechnol*, 28, 129-46 (2000)
135. Lutz, J., U. Noth, S. P. Morrissey, H. Adolf, R. Deichmann & A. Haase: *In vivo* measurement of oxygen pressure using ^{19}F-NMR imaging. *Adv Exp Med Biol*, 388, 53-7 (1996)
136. Jager, L. J., U. Noth, A. Haase & J. Lutz: Half-life of perfluorooctylbromide in inner organs determined by fast ^{19}F-NMR imaging. *Adv Exp Med Biol*, 361, 129-34 (1994)
137. Nunnally, R., P. Antich, P. Nguyen, E. Babcock, G. McDonald & R. Mason: Fluosol adjuvant therapy in human cancer: examinations *in vivo* of perfluorocarbons by F-19 NM. *Proc. SMRM 7th Meeting San Francisco*342 (1988)
138. Gewiese, B., W. Noske, A. Schilling, D. Stiller, K. Wolf & M. Foerster: Human eye: visualization of perfluorodecalin with F-19 MR imaging. *Radiology*, 185, 131-3 (1992)
139. Tadamura, E., H. Hatabu, W. Li, P. V. Prasad & R. R. Edelman: Effect of oxygen inhalation on relaxation times in various tissues. *J Magn Reson Imaging*, 7, 220-5 (1997)
140. Berkowitz, B. A., Y. Ito, T. S. Kern, C. McDonald & R. Hawkins: Correction of early subnormal superior hemiretinal DeltaPO (2) predicts therapeutic efficacy in experimental diabetic retinopathy. *Invest Ophthalmol Vis Sci*, 42, 2964-9 (2001)
141. Berkowitz, B. A., C. McDonald, Y. Ito, P. S. Tofts, Z. Latif & J. Gross: Measuring the human retinal oxygenation response to a hyperoxic challenge using MRI: eliminating blinking artifacts and demonstrating proof of concept. *Magn Reson Med*, 46, 412-6 (2001)
142. Zaharchuk, G., A. J. Martin, G. Rosenthal, G. T. Manley & W. P. Dillon: Measurement of cerebrospinal fluid oxygen partial pressure in humans using MRI. *Magnetic Resonance in Medicine*, 54, 113-121 (2005)
143. Zaharchuk, G., R. F. Busse, G. Rosenthal, G. T. Manley, O. A. Glenn & W. P. Dillon: Noninvasive oxygen partial pressure measurement of human body fluids *in vivo* using magnetic resonance imaging. *Academic Radiology*, 13, 1016-1024 (2006)
144. Kodibagkar, V. D. & R. P. Mason: Proton Imaging of Silanes to map Tissue Oxygenation Levels (PISTOL): a new tool for quantitative tissue oximetry. *Proc Intl Soc Magn Reson Med*, 14, 928 (2006)
145. Cassidy, S. L., A. Dotti, G. B. Kolesar, L. W. Dochterman, R. G. Meeks & H. J. Chevalier: Hexamethyldisiloxane: A 13-week subchronic whole-body vapor inhalation toxicity study in Fischer 344 rats. *Int J Toxicol*, 20, 391-9 (2001)
146. Dobrev, I. D., M. B. Reddy, K. P. Plotzke, S. Varaprath, D. A. McNett, J. Durham & M. E. Andersen: Closed-chamber inhalation pharmacokinetic studies with hexamethyldisiloxane in the rat. *Inhal Toxicol*, 15, 589-617 (2003)
147. Riess, J. G.: Overview of progress in the fluorocarbon approach to *in vivo* oxygen delivery. *Biomater Artif Cells Immobilization Biotechnol*, 20, 183-202 (1992)
148. Haase, A., J. Frahm, W. Hanicke & D. Matthaei: ^{1}H NMR chemical shift selective (CHESS) imaging. *Phys Med Biol*, 30, 341-4 (1985)
149. Zhao, D., L. Jiang, E. W. Hahn & R. P. Mason: Tumor physiologic response to combretastatin A4 phosphate assessed by MRI. *Int J Radiat Oncol Biol Phys*, 62, 872-80 (2005)
150. Wickline, S. A., A. M. Neubauer, P. M. Winter, S. D. Caruthers & G. M. Lanza: Molecular imaging and therapy of atherosclerosis with targeted nanoparticles. *J Magn Reson Imaging*, 25, 667-80 (2007)

Key Words: Oximetry, hypoxia, perfluorocarbons, MRI, ^{19}F, hexamethyldisiloxane, Review

Send correspondence to: Vikram Kodibagkar, Ph.D., Assistant Professor of Radiology, UT Southwestern Medical Center at Dallas, 5323 Harry Hines Blvd., Dallas, TX 75390-9058, Tel: 214-648-7612, Fax: 214-648-4538, E-mail: vikram.kodibagkar@utsouthwestern.edu

http://www.bioscience.org/current/vol13.htm